William & Mary
CHARTERED 1693

W&M ScholarWorks

Arts & Sciences Articles

Arts and Sciences

7-2023

Identification of Transient Radio Frequency Occlusion Events in Urban Environments

Margaret M. Rooney
William & Mary, margaret.m.e.rooney@gmail.com

Mark Hinders
William & Mary, hinders@wm.edu

Follow this and additional works at: https://scholarworks.wm.edu/aspubs

 Part of the Computer Sciences Commons

Recommended Citation

Rooney, Margaret M. and Hinders, Mark, Identification of Transient Radio Frequency Occlusion Events in Urban Environments (2023). *IEEE Access*, 11, 68051-68065.
https://www.doi.org/10.1109/ACCESS.2023.3292343

This Article is brought to you for free and open access by the Arts and Sciences at W&M ScholarWorks. It has been accepted for inclusion in Arts & Sciences Articles by an authorized administrator of W&M ScholarWorks. For more information, please contact scholarworks@wm.edu.

IEEE Access
Multidisciplinary | Rapid Review | Open Access Journal

Received 11 June 2023, accepted 26 June 2023, date of publication 5 July 2023, date of current version 11 July 2023.

Digital Object Identifier 10.1109/ACCESS.2023.3292343

RESEARCH ARTICLE

Identification of Transient Radio Frequency Occlusion Events in Urban Environments

MARGARET M. ROONEY AND MARK K. HINDERS
Department of Applied Science, William & Mary, Williamsburg, VA 23187, USA
Corresponding author: Margaret M. Rooney (margaret.m.e.rooney@gmail.com)

This work was supported in part by the U.S. Naval Research Laboratory, and in part by the Virginia Space Grant Consortium.

ABSTRACT We model the propagation of SHF OFDM signals around vehicles and buildings since these are the most common elements present in urban environments that could lead to complex radio frequency signal scattering. Scenarios involving temporary hidden node situations, which we term transient occlusion events, are simulated and compared to scenarios where a line of sight transmission event occurs. Sets of fingerprints generated from signals recorded in full-wave 3D finite difference time domain simulations of these two different types of situations are compared, and features in the fingerprints corresponding to the occlusion of a transmitted signal by a vehicle or a building are identified. The features we identify in the sets of fingerprints have promise to be used with machine learning algorithms to automate the detection of hidden nodes and to provide an understanding of node behavior in an environment. When combined with knowledge of the existence of scatterers such as vehicles and buildings in the immediate neighborhood of a device, this information can be exploited to determine the likelihood of obstructed vs. concluded transmissions for both civilian and military applications.

INDEX TERMS Wireless communications, SHF, 5G networks, FDTD simulations, electromagnetic modeling, electromagnetic scattering.

I. INTRODUCTION

In both cognitive radio networks and military applications, adapting wireless communications networks to utilize mmWave frequencies will create a host of operational challenges. Of these, one prominent concern is the scattering behavior of mmWave frequency signals in various environments. In urban environments consisting primarily of buildings and vehicles, it will likely become difficult to determine the difference between instances when a node has ended a transmission and when a node artificially appears to have concluded its transmissions, but is actually hidden behind an object in the environment. We call the latter scenario a transient occlusion event since these scenarios will often be temporary and will cause either a full or partial occlusion of the signal, resulting in a drastically reduced received signal strength. In cognitive radio (CR) networks, for instance, a device's assessment of spectrum usage might then indicate the existence of a vacancy in the spectrum, while in reality the channel might still be in use and an attempt by the CR to transmit on that channel would cause interference with the primary user. In military applications, the occlusion of a transmitter by a scatterer might result in the false conclusion that a jamming effort has been successful.

Here, we model the propagation of 9 GHz frequency signals around vehicles and buildings, since these are commonly encountered scatterers in urban environments and are likely to impact strongly the propagation paths of high frequency waves [1]. Scenarios with potential hidden node situations are simulated using high fidelity full-wave FDTD techniques and are compared to scenarios where a transmission event occurs in an environment void of any obstructions. Sets of fingerprints generated from signals recorded in the two different types of situations are compared, and features in the fingerprints corresponding to occlusion of a transmitted signal by a vehicle or a building are identified. The features we identify in the sets of fingerprints have promise to be used with machine learning algorithms to automate the detection of hidden nodes

The associate editor coordinating the review of this manuscript and approving it for publication was Cesar Vargas-Rosales.

This work is licensed under a Creative Commons Attribution 4.0 License. For more information, see https://creativecommons.org/licenses/by/4.0/

by recognizing various changes in a received signal as the progressive occlusion of a transmission. If the signals transmitted by the node under consideration are then no longer detected, such an event can be identified as a scenario where the node is still transmitting, but is either temporarily hidden by a scatterer moving into the area or has itself moved behind a permanent feature of the built landscape. When combined with knowledge of the existence of scatterers such as vehicles and buildings in the immediate neighborhood of a device, having an understanding of node behavior in a particular environment permits the determination of the likelihood of obstructed vs. concluded transmissions in both civilian and military applications.

II. BACKGROUND

Research into the development and operation of next generation networks has become an area of wide interest with the advent of 5G-New Radio (NR). Within the last two years, a multitude of publications has been added to the literature, focusing largely on constructing channel and ray-tracing models to predict path loss and signal strength in cluttered or highly trafficked indoor spaces [2], [3]. These include modelling the overall channel response for massive MIMO in crowded theaters and subway stations [4], and mapping the field strength and path loss in offices and corridors to model channel propagation of 38−73 GHz frequencies [5], [6], [7]. Others have applied machine learning techniques to experimental measurements to predict the path loss and coverage of 5G networks rather than employing empirical or deterministic models [8]. Although the training data consist of measurements made outdoors and around obstructions, they do not provide a complete understanding of the complex scattering undergone by high frequency signals. Rather than trying to predict path loss and signal strength, which would provide an understanding of whether a communications link could be reliably maintained, our work focuses on studying scenarios where a transmitted waveform becomes nearly indistinguishable from the ambient noise. The application of the dynamic wavelet fingerprint technique allows for transmissions to be identified in a received signal even when the signal strength drops significantly.

Since 5G networks are intended to be deployed reliably in both rural and urban areas, network models will need to take into account the complex scattering and multipath behavior of signals caused by obstacles in the environment. The most commonly used deterministic modelling methods include ray-tracing and finite difference time domain (FDTD) simulations. While FDTD simulations are more computationally intensive than ray-tracing implementations, they take into account complex scattering phenomena such as multipath, fading, and shadowing that are not inherent in ray-tracing methods. Combined ray-tracing/FDTD techniques have been used to predict electromagnetic field strengths in large scale urban areas and estimate the exposure levels that can be expected with varying numbers of network users [1]. The extent of the electromagnetic field exposure and the absorption of mmWave frequencies in biological tissues have also been studied using simulations based on the finite element method [9], the FDTD method [10], and a hybrid ray-tracing FDTD method [11].

Ray-tracing and FDTD methods have been leveraged to obtain the reflection and transmission coefficients of rough surfaces like wood and plasterboard in the 28 GHz frequency band in order to understand propagation behavior in indoor environments [12], while the FDTD method alone has been applied to determine the effect of the human body on indoor propagation at 26 GHz [13] and to predict path loss model parameters in an office environment at 28 GHz [14]. The FDTD method has also been applied to estimate the power distribution of networks using the 2.4 and 5.2 GHz bands, with a focus on predicting the strength of the signal that could be detected outdoors [15]. Network coverage and path loss of signals within these same frequency bands throughout office spaces have also been studied using ray-tracing simulations [16]. Several surveys discuss the work that has been conducted in channel modelling and estimation for 5G networks [17], [18], [19].

However, none of these publications considers the effects of scatterers in the environment on the transmitted waveform itself or the consequences of node and scatterer mobility. In this work, we examine the effects of scattering on actual OFDM signals, and identify scattering artifacts in the received waveform that indicate occlusion of a node by a feature of an urban environment.

The main contributions of this work are as follows:

1) We analyze and characterize the propagation of OFDM waveforms in complex scattering scenarios using full-wave 3D FDTD simulations, allowing us to explore the effects of scatterers and multipath, shadowing, and fading behaviors in the environment on the received waveform.
2) We convert raw time-domain waveforms to binary images using an amplitude agnostic wavelet-transform based technique, which allows us to consider the question of distinguishing between LOS and occluded transmissions as an image processing problem.
3) We exploit the strong frequency dependent behavior of RF scattering to identify features of a received signal fingerprint that correspond to occlusion of a transmitter.
4) We propose a framework for the prediction of transmitter occlusion events in urban environments that is based on the automatic detection of features related to scattering artifacts present in an occluded signal.

III. METHOD

First introduced by Kane S. Yee in 1966 as a method of finding a numerical solution to Maxwell's equations, the FDTD technique has in the decades since then been applied not only to electromagnetic scattering problems, but to acoustic and elastic scattering problems as well. Here, 3D FDTD simulations are used to model the propagation of 9 GHz frequency

signals around scatterers in the environment. A 9 GHz center frequency was chosen since it satisfied the Courant stability condition for the 0.5 mm spatial step used in the simulations, but we expect the results of our work to extend to frequencies above 9 GHz. The received signals recorded within the simulations are analyzed using the dynamic wavelet fingerprint (DWFP) technique, which has proven to be an effective way of identifying scattering artifacts in a recorded waveform [20].

The accuracy of the FDTD simulations we developed was verified by benchmarking simulation results using experimental measurements made with a set of universal software radio peripherals (USRPs). The experimental setup included two X310 USRPs equipped with UBX 160 MHz daughterboards and VERT 2450 omnidirectional antennae with 3 dBi gain. In our initial validation stage, experimental measurements made with the set of USRPs around a 6 cm radius metal cylinder were used to calculate the magnitude of the forward scattered wave and were compared to the corresponding scenario modelled in the FDTD computational space. Since the scattered field E^{scat} is defined as

$$E^{scat} = E^{total} - E^{inc} \tag{1}$$

where E^{total} and E^{inc} are the total electric field and incident electric field, respectively, we were able to determine the scattered wave component in both the FDTD scenario and in the physical scenario by measuring separately the total field and the incident field and then calculating the difference between the two.

To obtain experimental values, signals were collected every 5 cm along a horizontal axis running 10−45 cm radially from the outer edge of the cylinder to record the total electric field, and then the signals were recorded again without the cylinder while leaving the USRPs in the same positions to measure the incident wave. By subtracting the incident wave measurements from the total field measurements and then taking the absolute value, we were able to obtain approximate values for the magnitude of the scattered wave at various distances from the scatterer.

As indicated by the plot in Fig. 1, the normalized mean experimental values for the forward scattered wave measured with the USRPs correlated well with the normalized values calculated from the simulation results for the same scattering scenario.

The second stage of our FDTD verification work involved transmitting and recording 100 MHz bandwidth Gaussian pulse signals modulated to a center frequency of 2.5, 4.0, or 5.0 GHz with the USRPs in several different outdoor scattering scenarios. These environments contained a variety of objects with differing material properties and were compared directly to corresponding FDTD simulations. Propagation around six types of scatterers was studied: building corners, foliage in the form of trees and dense shrubs, a stationary food truck, a concrete pillar, a seated person, and a stone wall. In each scenario, the transmit and receive USRPs were placed between 0.5-2.0 m from the scatterer. Signals collected using

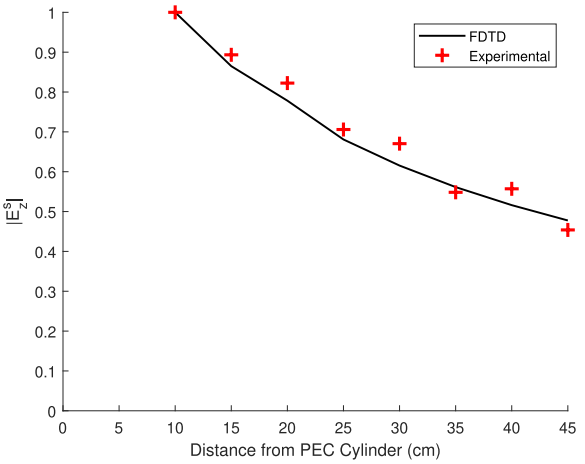

FIGURE 1. The normalized magnitude of the forward scattered wave plotted as a function of the distance of the receiving node from the outer wall of the 6 cm radius metal cylinder. The solid black line represents the FDTD results, and the red crosses represent the experimental values calculated from the USRP data.

the USRPs were compared to the FDTD results using the DWFP method. Using image processing techniques, features relating to the shape, complexity, and area covered by the fingerprints were calculated from each significant object in the sets of fingerprints and plotted as a function of time, and the correlation between the sets of feature plots was analyzed. Doing so ensured that our simulations correctly characterized interactions between signals and various scatterers commonly encountered in outdoor environments. To perform a comparison between simulated wave propagation and physical signal propagation, simulations were run in which the Gaussian pulse input was transmitted and recorded at the Rx node several times over the course of a simulation. This allowed for the identification of consistent patterns across sets of signals with greater certainty than would have been possible by comparing a single simulation-derived waveform to a series of physical signals.

In order to model communications similar to 5G-NR networks, the simulations presented here used as the input signal a segment of a 500 MHz bandwidth orthogonal frequency division multiplexing (OFDM) packet that was resampled according to a time step satisfying the Courant stability condition of the FDTD code, making it suitable for use within a simulation with a 5 mm spatial step. By using a windowed segment of an OFDM modulated packet as the input signal for these simulations, the fingerprint features identified as being associated with particular scattering scenarios will be consistent with those that are likely to occur in actual deployed 5G-NR networks, since these networks will consist of OFDM-based waveforms [21], [22]. Since the OFDM waveform being used as the input signal had a 500 MHz bandwidth, it was modulated to a 9 GHz center frequency in order to ensure that all the frequency components of the modulated signal remained under the 10 GHz frequency limit set by the spatial resolution of the FDTD simulation.

The OFDM waveform modulated to a 9 GHz carrier frequency results in an input signal spanning the 8.75-9.25 GHz area of the spectrum, which is within the resolvable frequency range of simulations using a 5 mm spatial step. In order to ensure that the features identified in sets of fingerprints were actually indicative of transient occlusion events and did not occur just for a specific OFDM symbol, three input signals were created from randomly selected sections of the resampled 500 MHz bandwidth OFDM packet. Each scattering scenario was then modelled three times, once for each of the input signals.

A set of ten scattering scenarios were created to simulate transient occlusion events in urban surroundings. Five of these scenarios modelled transmission and reception of OFDM signals when two nodes were positioned a meter above the ground at various points on opposite sides of a truck, and the other five scenarios modelled situations where the two communicating devices were located near or on adjacent sides of a building. LOS communication scenarios with the Tx and Rx nodes in the same positions as in the ten NLOS simulations were also modelled to compare against the scattering scenarios, allowing for inferences about how transient occlusion events may be distinguished from concluded LOS transmissions to be made.

IV. SCATTERING FROM A VEHICLE

In order to explore the modifications to the received signal that are caused by trucks, a series of simulations were executed modelling propagation of an OFDM waveform around a vehicle. In these simulations, the Tx and Rx nodes were placed at different points around a CAD model of the front half of a truck, so that the full size of the simulation space was $3.5 \times 3.5 \times 2.5$ m and consisted of nearly 250 million grid points. Using a high performance computing (HPC) cluster, simulating the transmission and reception of an approximately 8000 sample OFDM signal in this space required approximately 180 hours to complete. Simulations of 12,000 time steps, which allowed for the entirety of the transmitted signal to be recorded at the receive node several meters away, required 68−72 GB of memory on an HPC subcluster. For each of the scattering scenarios we modelled, we also simulated signal propagation in the corresponding LOS scenario. By comparing the LOS and NLOS situations, we were able to determine which features in the received signal were related to the presence of certain scatterers in the environment.

In the first simulation space, the nodes were placed on opposite sides of a truck, 3.0 m apart, each 1.5 m down from the front of the vehicle and 0.5 m from the side of the vehicle as shown in Fig. 2. For the second propagation environment, the Tx node was positioned 0.5 m from the front right corner of the truck while the Rx node remained where it had been located in the previous scenario such that the separation distance was increased to 3.15 m. The next NLOS simulation had the Tx node moved to be in line with the outermost part of the front fender, with the Rx node still 1.5 m down the side of the truck, resulting in a node separation of 3.35 m. Similar

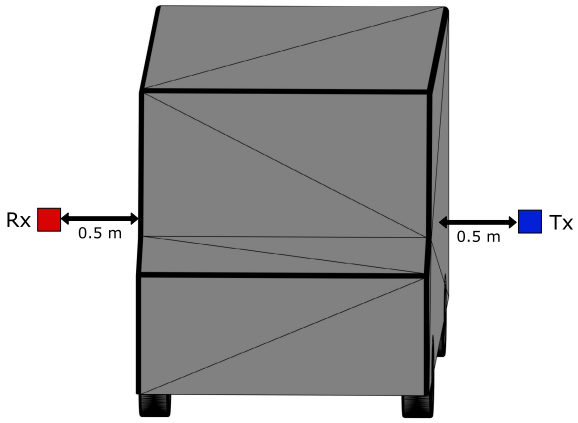

FIGURE 2. Configuration of the simulation space used to model transmitter occlusion by a vehicle, Scenario 1.

to the composition of the first simulation space, the fourth NLOS scenario had the nodes 3.0 m apart and 0.5 m from the front of the vehicle, while in the last NLOS model the Tx and Rx nodes were positioned at the front corners of the hood of the truck. In all of the simulations concerning scattering from a vehicle, the nodes were set at a height of 1 m above the ground. The electromagnetic constitutive parameters for the metal exterior of the vehicle were set as $\epsilon_r = 1.0$, $\mu_r = 1.0$, with electric conductivity $\sigma = 1.0 \cdot 10^7$ S/m [23], [24]. For each of the three OFDM input signals, five simulations were run with the Tx/Rx nodes placed at the described positions on either side of the vehicle.

V. SCATTERING FROM A BUILDING

After modelling occlusion events featuring a vehicle as the scatterer, scenarios involving OFDM signal propagation near and around building corners were modelled. In each of the five scattering scenarios, the simulation space contained a $2.0 \times 2.0 \times 1.0$ m corner of a brick building exterior, with 20cm thick walls and an air-filled building interior. The first two NLOS simulations covered an area of $2.5 \times 2.5 \times 1.0$ m, while the other three consisted of a $3.0 \times 5.0 \times 1.0$ m simulation space, resulting in grids of between 25 million and 60 million cells. The run times for these simulations averaged 25−60 hours, and required 12−30 GB of memory. The electromagnetic constitutive parameters for the face of the brick building were set as $\epsilon_r = 3.58$, $\mu_r = 1.0$, with electric conductivity $\sigma = 3.8 \cdot 10^{-}2$ S/m [24], [25]. As with the vehicle scattering simulations, sets of LOS communications were modelled using node configurations identical to those in the five NLOS scenarios.

For the first occlusion simulation, the nodes were arranged on adjacent sides of the building at a distance of 1.5 m from the corner and 0.25 m away from the wall, so that a diagonal distance of approximately 2.5 m existed between them as shown in Fig. 3. In the following scattering scenario, the Rx node remained at the point 1.5 m from the corner, while the Tx node was located at the corner so that the nodes

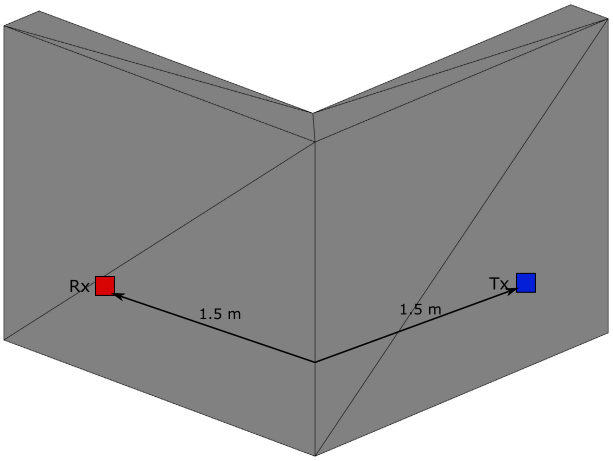

FIGURE 3. Configuration of the simulation space used to model transmitter occlusion by a building, Scenario 1.

were 1.75 m apart. In the last three NLOS scenarios, the Rx node was set 2 m out from the wall and 1.5 m down from the corner. The Tx node in the third scattering environment was placed 2 m away from the corner towards the receiver so that it was 2.0 m away from the Rx node. In the next model, the Tx node was moved close to the corner, so that the distance between the nodes increased to just under 3.0 m. In the final simulation environment, the Tx node was positioned further down along the wall so that the direct path of communication between the nodes was occluded by the building.

VI. ANALYSIS OF RECEIVED SIGNALS USING THE DWFP

The recorded physical layer signals were filtered and analyzed using the dynamic wavelet fingerprint (DWFP) method, which uses a wavelet transform to convert time domain signals into two-dimensional binary images resembling sets of fingerprints. This method has been used successfully over the last decade to analyze a wide range of signals, including structural health monitoring and flaw detection [26], radio-frequency identification clone detection [27], analyzing topics extracted from Twitter [28], [29], and communicating through ice in the Arctic [30].

Wavelets are sets of basis functions that were developed to provide compact local support for non-stationary, non-periodic signals. Since local signals vanish outside a short interval of space or time, representing such signals using global bases would require extreme cancellation, and achieving a reasonable accuracy would necessitate many additional terms of the Fourier series. Allowing the wavelet parameters to change continuously supplies the requisite support for an accurate representation of the signal. Under the wavelet transform, the signal is decomposed into a series of expansion coefficients useful for signal filtering, denoising, and reconstruction applications. Wavelets within the same family are orthogonal, which facilitates computation of the expansion coefficients.

The continuous wavelet transform of a continuous function $s(t)$ is defined as

$$C(a, b) = \int_{-\infty}^{+\infty} s(t)\psi_{a,b}(t)dt, \tag{2}$$

where $\psi(t)$ represents the mother wavelet and $\psi_{a,b}(t)$ is given by

$$\psi_{a,b}(t) = |a|^{-1/2}\psi\left(\frac{t-b}{a}\right). \tag{3}$$

The constants $a, b \in \mathbb{R}$ are the scaling and translation parameters, respectively, and each pair (a, b) relates to one value of the integral $C(a, b)$. The translation parameter corresponds to the time localization of ψ, which contains time information that is generally lost during Fourier analysis, while the scaling parameter corresponds to the sizing of the mother wavelet. The scale value is associated with the frequency composition of the signal $s(t)$, where large a values accentuate low frequency content and small a values relate to high frequency content.

By discretizing the scaling and translation parameters, the computational expense of calculating the wavelet transform decreases. Rather than evaluating the integral in (2) for all values of a and b, computations are only carried out for discrete nodes. The discrete wavelet transform requires both the wavelet function and a scaling function, which together fully cover the frequency content of a signal. These functions provide the basis for iterative signal decomposition where low frequency components, referred to as approximations, are detected by the low-pass scaling function, and high frequency components, or details, are detected by the high-pass wavelet function. Under this decomposition scheme, details from the first several levels can be filtered out prior to implementing the reverse transform to remove unwanted noise from the signal. The DWFP algorithm uses a wavelet transform to denoise and convert time domain signals into two-dimensional black and white images resembling sets of fingerprints. Spatial features extracted from these fingerprints can be incorporated into feature vectors and used for the development of machine learning classifiers.

Under the DWFP method, the CWT in (2) is evaluated for finite ranges of the scale and translation parameters, producing an array of coefficients $C(a, b)$. The coefficient array $C(a, b)$ is then normalized so that for all $c \in C(a, b)$, $-1 \leq c \leq 1$. After being normalized, $C(a, b)$ is segmented into slices which are then projected onto the time-scale plane and labelled using an alternating pattern of ones and zeroes. The final result is a binary image $I(a,b)$, where the pixel dimensions a and b are the wavelet scale and translation factors, respectively. A more detailed explanation of the DWFP technique and a full derivation of the equations may be found in [32].

All simulation results have been analyzed using the DWFP technique, which allows us to draw comparisons between signals of vastly differing magnitudes and requires no *a priori* knowledge of the parameters of the transmitted waveform.

All signals were denoised and converted to sets of fingerprints using the Symlet 6 family of wavelets. Since the bandwidth of the OFDM signal was 500 MHz, the fingerprints were created using a maximum wavelet scale of 1000 to exhibit the broad frequency content of the signal. Figures 4 and 5 contain examples of the sets of fingerprints generated from two sets of simulations.

A. USING PIXEL DENSITY TO DIFFERENTIATE BETWEEN OCCLUSION EVENTS AND LOS TRANSMISSIONS

In each set of fingerprints generated from the pre-transmission OFDM signals there are areas where several consecutive individual fingerprint objects do not span the entire wavelet scale (y-axis), but contain frequency content primarily within the highest end of the bandwidth range that is represented by the lowest scale region. These same sparse high scale areas are also present in the sets of fingerprints generated from the results of the various LOS scenario simulations. However, a comparison between the LOS scenario fingerprints and the occluded signal fingerprints shows that when an OFDM signal interacts with a scatterer, whether a building corner or a vehicle, the set of fingerprints generated from the received signal is more uniformly dense over the full wavelet scale than it is in the absence of a scatterer, because of diffraction and differing arrival times of multipath components. After processing the data from all simulations and generating sets of fingerprints from the received signals, the pixel density was plotted for different scale ranges as a function of time in order to highlight the differences between the localized frequency content of received LOS transmissions and occluded signals.

The pixel density refers to the quantity of one-valued pixels in a certain area of a set of fingerprints. Each set of fingerprints is defined as a binary image $I(a,b)$ where the pixel dimensions a and b are the wavelet scale and translation factors, respectively, and all pixel values are either zero or one. Since the wavelet scale is related to signal frequency, extracting the pixel density feature from a set of fingerprints provides information about the localized frequency content of a particular section of a signal relative to the entire signal. This feature was calculated by first subdividing the scale axis of the set of fingerprints into horizontal slices. Since the wavelet scale for the sets of OFDM signal fingerprints ranges from $a = 1 : 1000$ and most of the differences between transient occlusion event signals and LOS signals were observed in the highest scale area, the scale dimension of the fingerprint array was divided into five bands of 200 scale values. Then for every time step, the pixel density in each of the five scale ranges was determined. These values were smoothed and plotted as a function of time to facilitate comparison between simulation results. Figures 6–7 contain plots of the pixel densities for the highest wavelet scale ranges of the sets of fingerprints generated from the simulation results.

As the transmitted signal becomes more fully occluded, the pixel density in the set of fingerprints becomes more highly concentrated across all time steps in the wavelet scale range from $a = 801 : 1000$, which is the lowest area of the frequency range covered by the OFDM signals. This phenomenon is well illustrated by the set of fingerprints in Figs. 4–5 and the smoothed pixel density plots in Figs. 6–7. In each of the other scale bands, the pixel density features extracted from the LOS and occluded signals align closely. There are some scenarios where the $a = 601 : 800$ scale range exhibits the same differentiation between LOS and NLOS transmissions as the highest scale range does, but these are often not as pronounced and the sparse regions span only a couple hundred time steps. An automatic detection algorithm was then developed to locate these sparse high scale areas by identifying regions where the pixel density did not exceed 15% of the wavelet scale band for a span of at least 400 time steps. These thresholds are both modifiable parameters within the function, and were defined based on the pre-transmission signal fingerprint characteristics. After identifying sparse high scale regions in the set of fingerprints, these areas were bounded in the plots to facilitate quantification by the user. In the smoothed density plots shown in Figs. 6–7, the detected areas devoid of high scale content are bounded by solid red lines.

VII. RESULTS AND DISCUSSION

As the wavelength of a signal decreases, its propagation behavior becomes more sensitive to obstacles in the environment, and the likelihood that the received waveform exhibits artifacts resulting from interactions with those scatterers rises. Therefore, it might prove increasingly challenging in some environments to distinguish between occasions when a transmission has concluded and when it has simply become difficult to detect over ambient noise due either to a node's mobility or to the arrival of a scatterer in the environment. We have explored the application of the DWFP technique to results from simulations modelling the described occurrences with the intention of differentiating between these scenarios.

Prior simulations highlighting the frequency dependency of scattering environments have shown that increasing the carrier frequency from 5 GHz to 10 GHz resulted in a received signal exhibiting significantly more complex diffraction and multipath components. In these simulations, a truck was inserted into the simulation space after one pulse had been transmitted with LOS communications, so that the body of the truck was then blocking the direct path between the two nodes. Following the arrival of the scatterer, a second pulse was transmitted. The top plots in Figs. 8a–b show the received time domain signals for the 5 and 10 GHz center frequencies, respectively. The first pulse, which was received prior to the arrival of the vehicle, is immediately evident, while the second pulse, the reception of which was impeded by the scatterer, is not easily visible in the time domain. Beneath the time domain plots are sets of fingerprints generated from the outlined segments of the received signal. In both signals, the second pulse is visible and comparable to the first pulse after being converted to the fingerprint domain. The sets of fingerprints show that while the pulses carried on both the 5 GHz and 10 GHz frequency signals were perceptible at

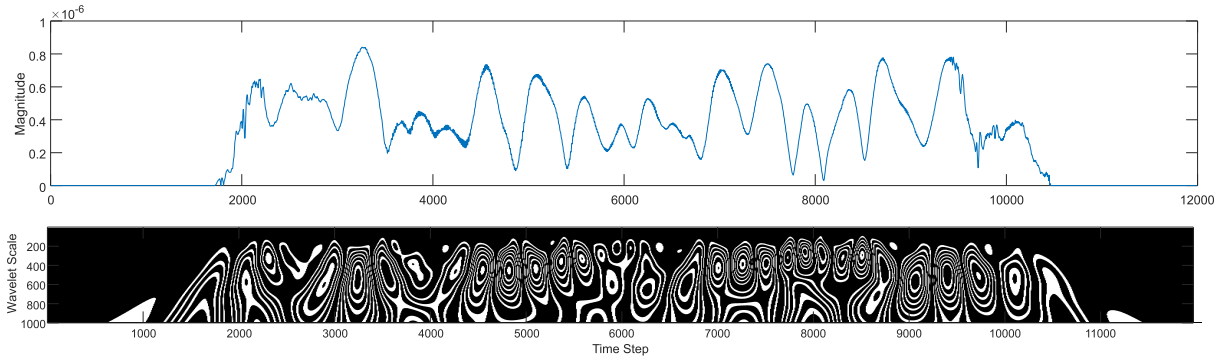

(a) NLOS scenario

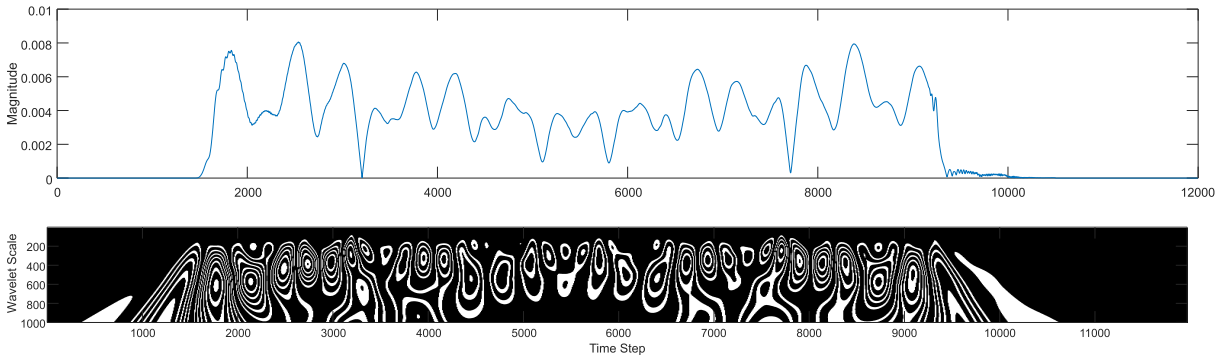

(b) LOS scenario

FIGURE 4. **Time domain plots and sets of fingerprints generated for the received signal recorded in the vehicle scattering scenario 1 simulation and the corresponding LOS scenario using OFDM signal 1.**

the Rx node on the opposite side of the vehicle, the pulse that had been modulated to the 10 GHz center frequency exhibited stronger scattering artifacts after having been occluded by the metal truck.

In order to perform a quantitative comparison of the impact of increased frequency on the scattering behavior of an RF waveform, the second received pulses in Fig. 8 from the simulations were analyzed using the DWFP. Since the signals recorded within the simulations are noiseless, the occluded transmission is still visible in the time domain if the area of the waveform containing that pulse is enlarged sufficiently, as shown in Fig. 9 for the 5 and 10 GHz signals, respectively. The ridge count feature of the sets of fingerprints were extracted for each pulse, and a comparison between graphs of the number of ridges present over time were created. The ridge count metric highlights the more pronounced difference in arrival times of the multipath components of the 10 GHz signal, indicated by the dual peaks in the ridge count feature plot, and revealing the imbrication of the scattered components of the received waveform. At the lower center frequency of 5 GHz, the scattering artifacts are not evident. Based on these results emphasizing the increased impact of the scattering environment on higher frequency RF signals, we concluded that this heightened scattering behavior would be integral to the identification of occlusion scenarios.

All the scattering simulations modelled situations where a transmission was to some degree occluded or influenced by a feature of the built environment. The type of occlusion event was determined according to the length of the minimum NLOS path between the Tx and Rx nodes, as defined in Table 1. In the vehicle simulations, scenarios 1 and 2 were considered full occlusion situations since the combined distance of the two nodes from the front of the vehicle was equal to or greater than 2 meters. When the nodes were configured such that the combined distance from the corners of the front fender was between 1.0 and 1.5 m, the scenario was labelled a partial occlusion event. Therefore, this label was applied to vehicle scattering simulations 3 and 4. The propagation model in which the nodes were placed precisely at the front corners of the vehicle, simulation environment 5, was defined as a slight occlusion event. In the building corner simulations, the first and fourth scenarios were labelled as partial occlusion events. The shortest NLOS paths between the two nodes in these simulation spaces were approximately 3 meters. Scenario 2 was considered a slight occlusion situation since there was a LOS path between the transmitter and receiver, but both nodes were within 0.25 m of the building, allowing for the creation of a strong scattering environment. No direct occlusion of either node was apparent in scenario 3, but the presence of the building corner in the vicinity would be sufficient to induce a scattering environment. Finally, the

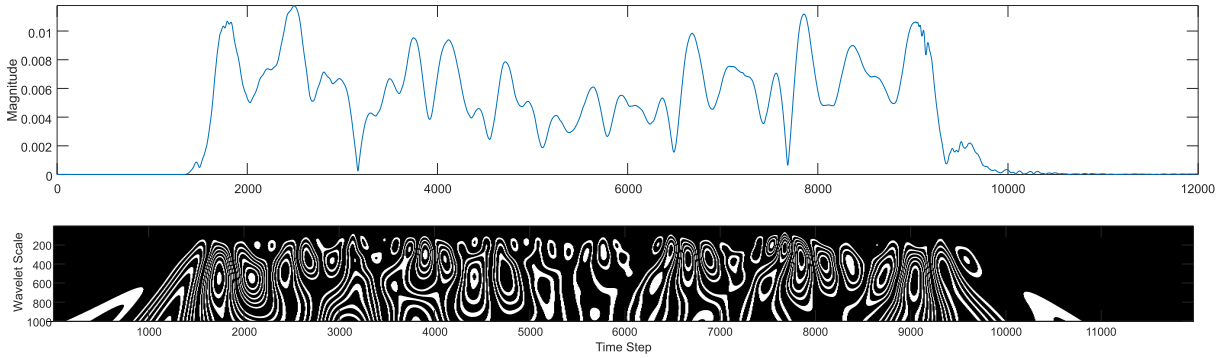

(a) NLOS scenario

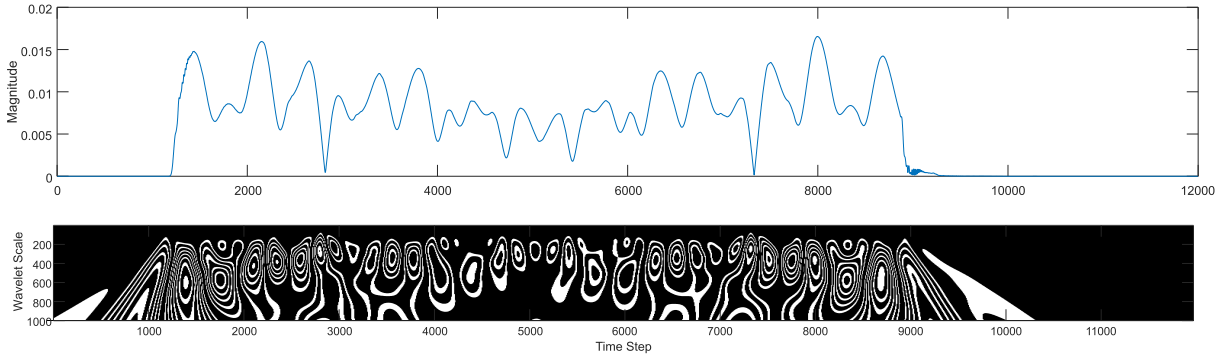

(b) LOS scenario

FIGURE 5. Time domain plots and sets of fingerprints generated for the received signal recorded in the building corner scattering scenario 1 simulation and the corresponding LOS scenario using OFDM signal 1.

TABLE 1. Definitions of the types of occlusion events modelled in the 3D FDTD simulations.

Type of occlusion event	Minimum NLOS path
Full	Greater than 4.5 m
Partial	3.0−4.0
Slight	Less than 2.5 m

fifth building corner scattering scenario was identified as a full occlusion sccenario, since the shortest NLOS path between the nodes exceeded 4.5 m and the transmitter was 2 m away from the building corner. All environments where the nodes were able to maintain a clear path of communication in the absence of nearby scatterers were considered LOS simulations.

Since the first part of the DWFP algorithm filters the noise from the waveform under consideration, the set of fingerprints produced for an OTA transmission received under LOS conditions match closely those produced for the pre-transmission signal. Therefore, we were able to conclude that features in the transient occlusion event signal fingerprints that are not present in the LOS signal fingerprints are the result of interactions between the transmitted signal and the built environment. Because high frequency signals scatter more strongly than lower frequency components and are more susceptible to rapid attenuation, we anticipated more prominent lower frequency reflections and multipath artifacts in signals received during occluded transmission scenarios as well as in instances where the distance between communicating nodes was several meters. Signals with shorter wavelengths result in lower levels of diffraction [31], so NLOS signals recorded at a receive node are less likely to contain the complete range of high frequency content that comprised the transmitted signal.

Our analysis of the signals obtained from modelling transient occlusion events using the smoothed pixel density feature indicated that the highest frequency components scatter more strongly than the lower frequency content, and in the case of scattering from a building corner, are absorbed by the material. This conclusion is reinforced by the visualisation of the waves propagating in the simulation spaces, shown in Figs. 10−11, where the wavelengths of the signals at the receive node are slightly longer than those measured at the transmitter. Therefore, at the receive node, the lower frequency content is more dominant. A comparison between the highest frequency (lowest scale) content in the transient occlusion event and LOS scenarios shows that some of the higher frequency content is lost after the wave propagates around the side of the building. The visualizations of the z-component of the electric field in Figs. 10−11 also convey the significant spatial dependence of scattering in the 9 GHz frequency band: a shift of only a few centimeters in any direction may move a device into an area of greater constructive or destructive interference.

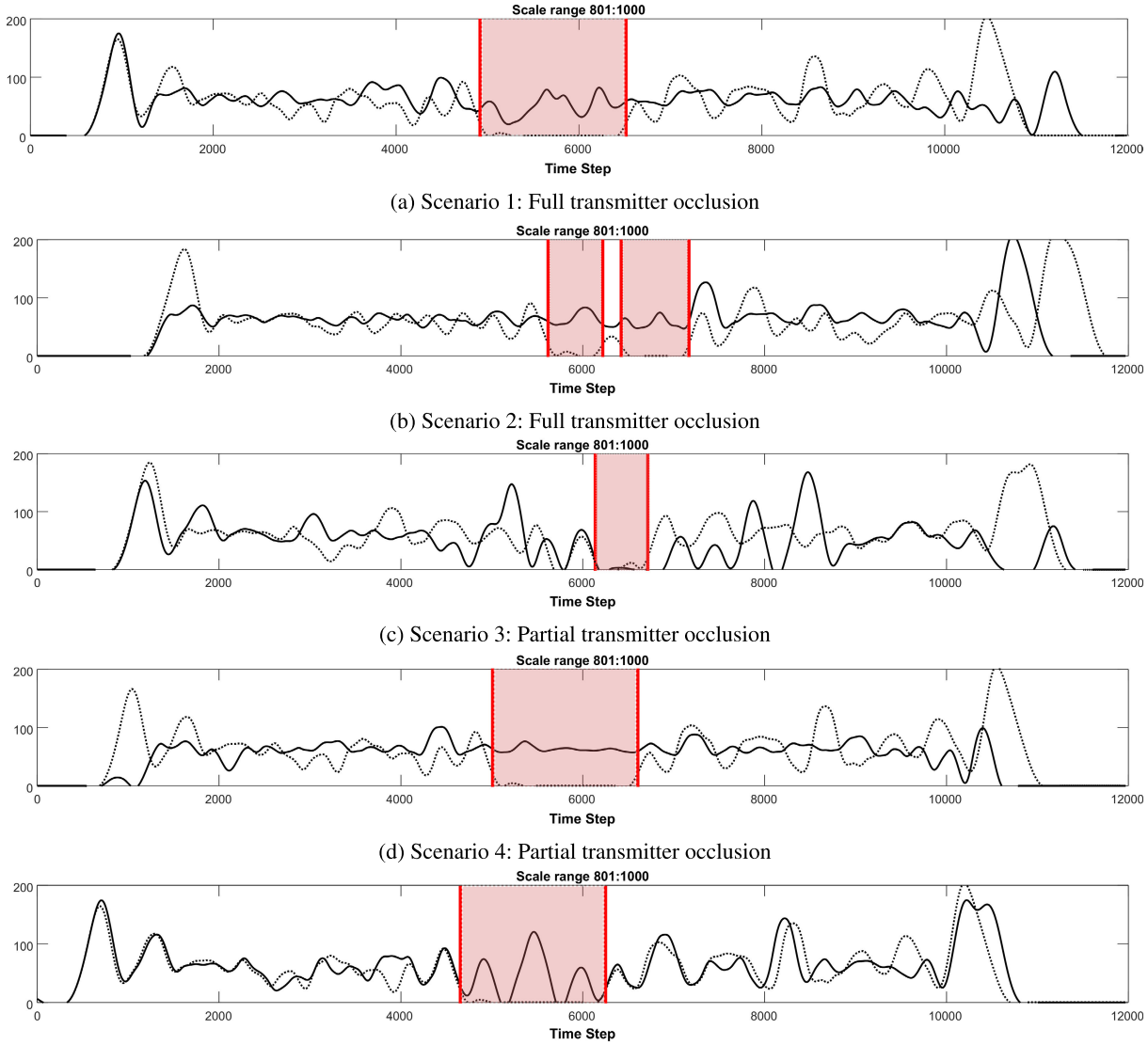

(a) Scenario 1: Full transmitter occlusion

(b) Scenario 2: Full transmitter occlusion

(c) Scenario 3: Partial transmitter occlusion

(d) Scenario 4: Partial transmitter occlusion

(e) Scenario 5: Slight transmitter occlusion

FIGURE 6. Plots of the smoothed pixel density feature for all five vehicle scattering scenarios using the first OFDM input signal. The solid line represents the results from the transient occlusion event simulation, while the dotted line represents the results from the LOS scenario. The shaded area bounded by the solid red lines indicates automatically detected areas devoid of high scale content in either the LOS or NLOS signal.

For the building corner simulations, the scenarios where there are no anticipated exclusively high frequency content areas may be regions of higher interference which are shown in the stills from the propagation models. Scattering is also highly spatially dependent, so it may be possible that by moving even several centimeters away, results more consistent with those expected would be obtained. In addition, the diffracted and multipath components present in the received signal are often offset by several hundred to tens of hundreds of time steps depending upon the NLOS distance between nodes. As a result of these scattering phenomena, it can be inferred that segments of the signal spanning the full frequency range may be superimposed on subsequent sections of the signal when they are recorded at the receive node. In some instances, these superpositions may coincide with solely low scale regions, while others may coincide with areas where the frequency content covered the full frequency bandwidth.

In the simulation results for vehicle scattering scenario 1, one sparse high scale area was identified in each of the three LOS signals, an example of which is highlighted by the shaded area in Fig. 6a. Of the three total sparse areas detected in the LOS simulation results, none were present in the transient occlusion event model results. The number of detected sparse areas in the LOS signals corresponding to vehicle scattering scenario 2 increased to five since some of the original regions with no high scale content were split into two sections by a small object in the binary image that exceeded the low pixel density threshold of the detection

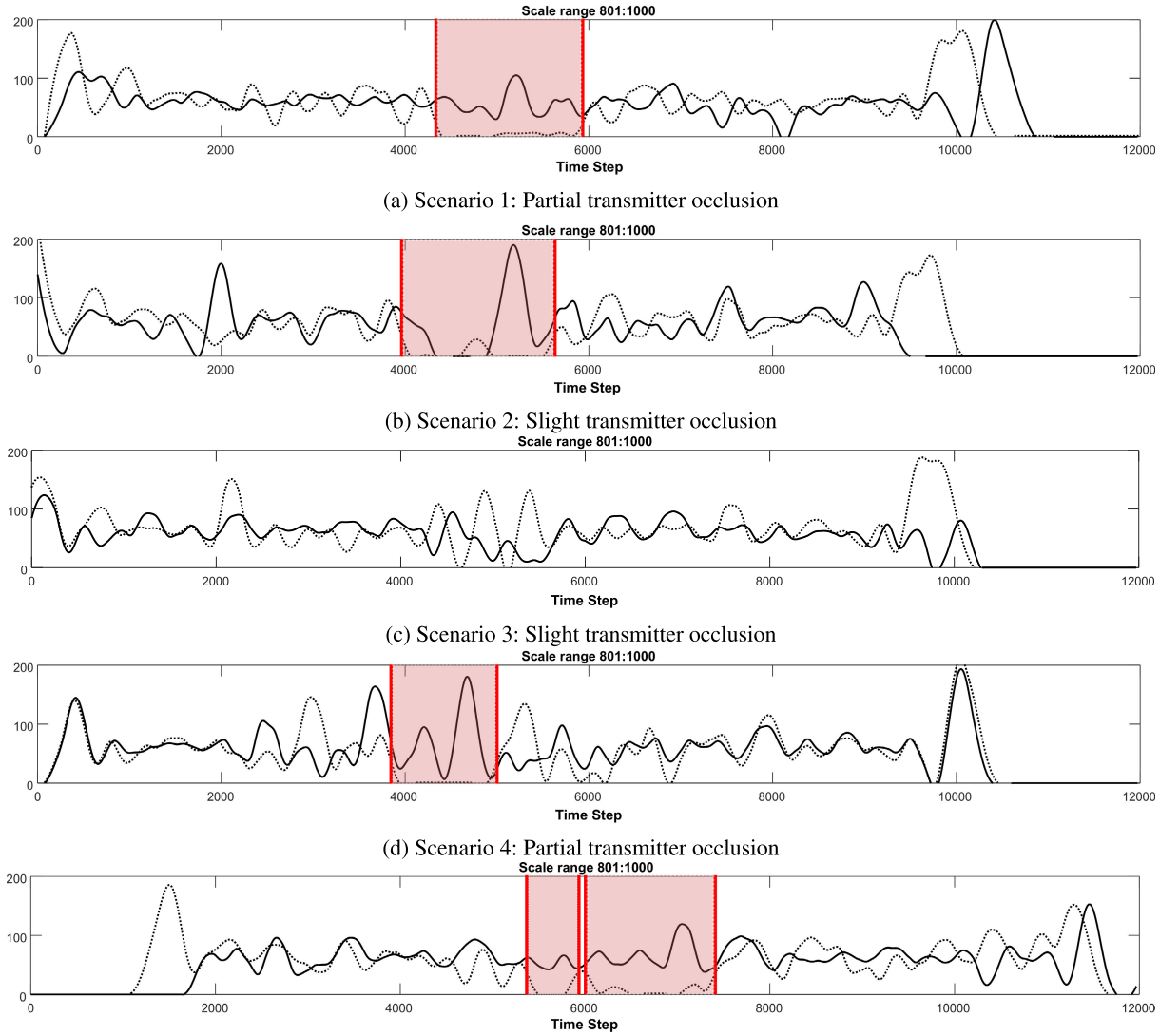

(a) Scenario 1: Partial transmitter occlusion

(b) Scenario 2: Slight transmitter occlusion

(c) Scenario 3: Slight transmitter occlusion

(d) Scenario 4: Partial transmitter occlusion

(e) Scenario 5: Full transmitter occlusion

FIGURE 7. Plots of the smoothed pixel density feature for all five building corner scattering scenarios using the first OFDM input signal. The solid line represents the results from the transient occlusion event simulation, while the dotted line represents the results from the LOS scenario. The shaded area bounded by the solid red lines indicates automatically detected areas devoid of high scale content in either the LOS or NLOS signal.

algorithm. Once again, no sparse high scale regions were identified in the NLOS signals, as exhibited in Fig. 6b. The results for vehicle scattering scenarios 3 and 4 (examples provided in Figs. 6c and 6d, respectively), both of which were labelled as partial occlusions, showed that one quarter of the number of sparse regions detected in the LOS signals could be observed in the signals recorded while a scatterer was occluding the transmission. Finally, in the fifth vehicle scattering model, labelled a slight occlusion scenario based on the node configuration with respect to the scatterer, two sparse areas were observed in the NLOS signal while three similar regions were evident in the LOS signal. An example of these results using the first OFDM input signal is shown in Fig. 6e. Thus, it could be inferred that as the occlusion of the transmitted signal by a vehicle became more substantial, the number of anticipated primarily high scale content areas in the associated set of fingerprints decreased.

The models where the transmitted signal was interacting with a building corner demonstrated similar quantities of detected sparse high scale areas for varying levels of occlusion. An example of the results for building corner scenario 5, which modelled a full occlusion of the transmitted signal, are provided in Fig. 7e. Three areas were identified in the LOS signals as having no high scale content, while no such regions were detected in the NLOS signal. The results from the partial occlusion events simulated in scenarios 1 and 4 (example results provided in Figs. 7a and 7d) each contained two detected sparse high scale areas in the smoothed pixel

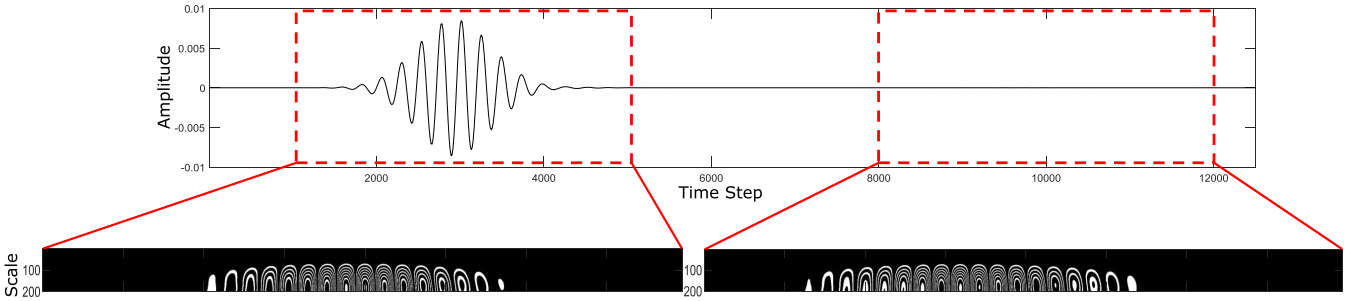

(a) Received pulse modulated to a 5 Ghz signal

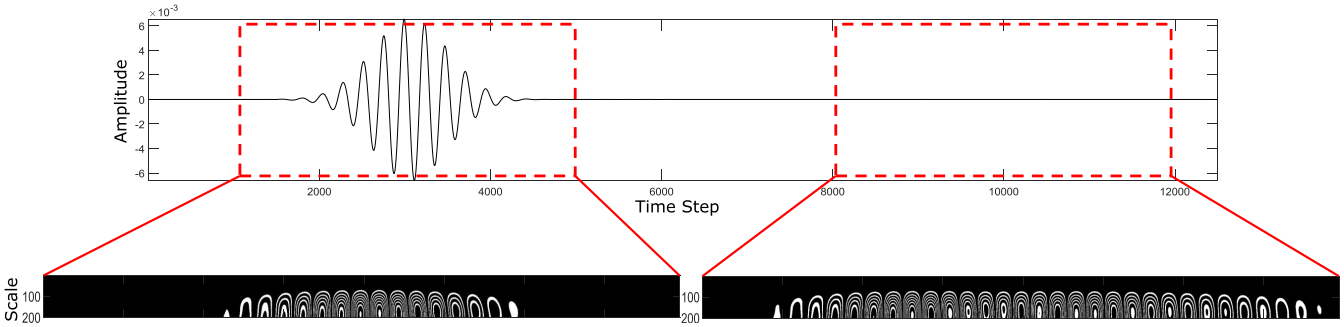

(b) Received pulse modulated to a 10 Ghz signal

FIGURE 8. **Received signal for a simulation where LOS communication between two nodes was interrupted by the arrival of a truck. The pulses in the time domain and in the fingerprint domain are outlined in red. The transmitted signal had been modulated to a 5 GHz center frequency (a) and to a 10 GHz center frequency (b).**

density plots. While the automatic detection algorithm identified three sparse areas in the corresponding LOS signals for scenario 1, a fourth probable region exists that was centered around time step 5500 of the first LOS signal. Similarly, although only two sparse areas were definitively identified in the pixel density plot for the scenario 4 LOS results, two additional probable sparse regions are centered around time steps 6000 and 7000 of the first and third LOS signals, respectively. The characteristics of these regions were just outside the bounds of the parameters set to indicate positive identification of a sparse high scale area. Building corner scenario 2 characterized slight transmission occlusion, and as shown by the pixel density plot from one set of the simulations in Fig. 7b, two sparse high scale areas were detected in the occluded signals while three such regions were located in the LOS simulation results. Although the third building corner simulation environment did enable LOS communication between the transmitter and receiver, the presence of the building corner near the two nodes created a scattering environment, so this was labelled a potential NLOS scenario. The pixel density plots showed that one area of sparse high scale content was identified in the NLOS signal fingerprints, while three sparse regions were found in the LOS signal fingerprints.

While this distinction between the frequency content comprising specific regions of received occluded and LOS signals is apparent in the fingerprint domain, it would not be obvious from analyzing the time domain signals alone that the frequency content of the signal was altered as a result of interactions with a scatterer. Though changes in the magnitude and signal strength of a received signal would be detected, this alone would not be sufficient to make inferences about a node's surroundings, since such changes could merely be the result of an intentional reduction in transmission power or of increasing distance between nodes in a LOS environment. Applying the DWFP technique to received signals has allowed us to identify features within the sets of fingerprints which have promise to be used with machine learning algorithms to automate the prediction of imminent transient occlusion events in urban settings.

If we recognize that changes in the set of fingerprints generated for a received signal correspond to transient occlusion events, then if the signal becomes at any point impossible to detect at the receiver, one can infer that the transmitter has become completely occluded by an element in the environment. However, by monitoring these gradual changes, a system should be able to indicate that the absence of a transmitter is not permanent and that the receiver can expect the transmissions to become detectable again imminently. Conversely, if transmissions seem to have concluded and no evidence of partial or gradually increasing levels of occlusion are identified in the fingerprints of the recently recorded signals, the receiver may surmise that the transmitting node has intentionally ceased communications.

Since transmitted packets will contain many OFDM symbols in the payload, we expect fingerprints generated from

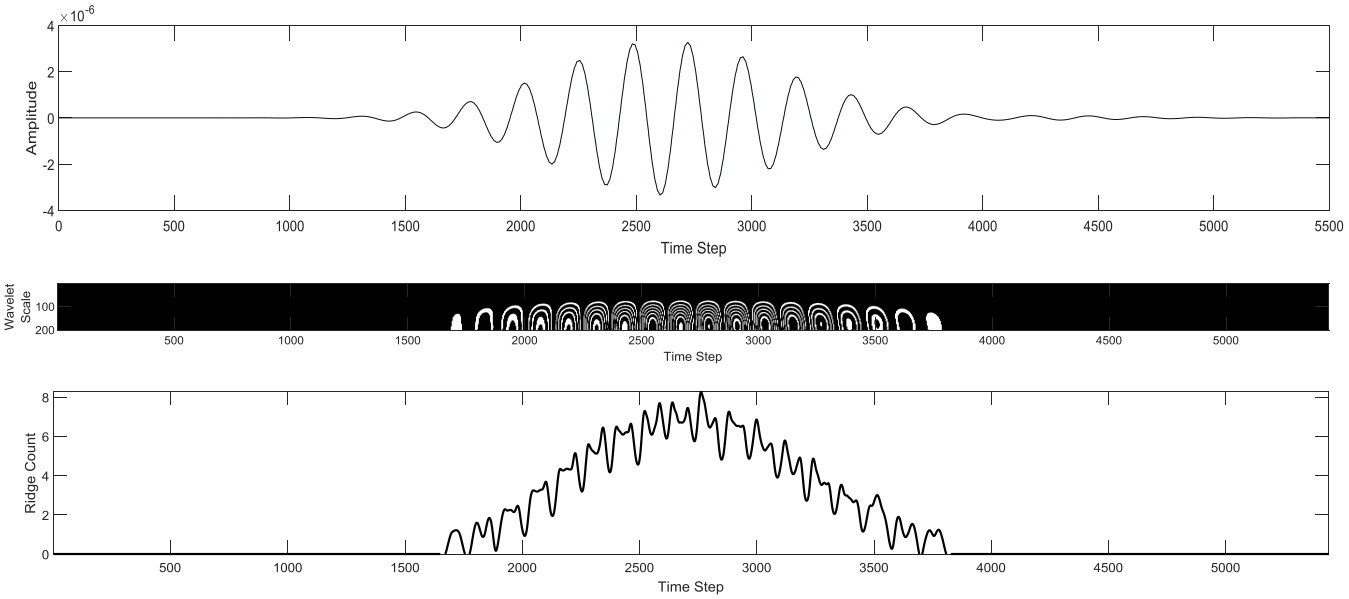

(a) (Top) The time domain plot of the second pulse in the received signal for the 5 GHz frequency simulation. (Middle) The set of fingerprints generated for this segment of signal is shown directly below the time domain plot. (Bottom) A plot of the ridge count feature for the set fingerprints.

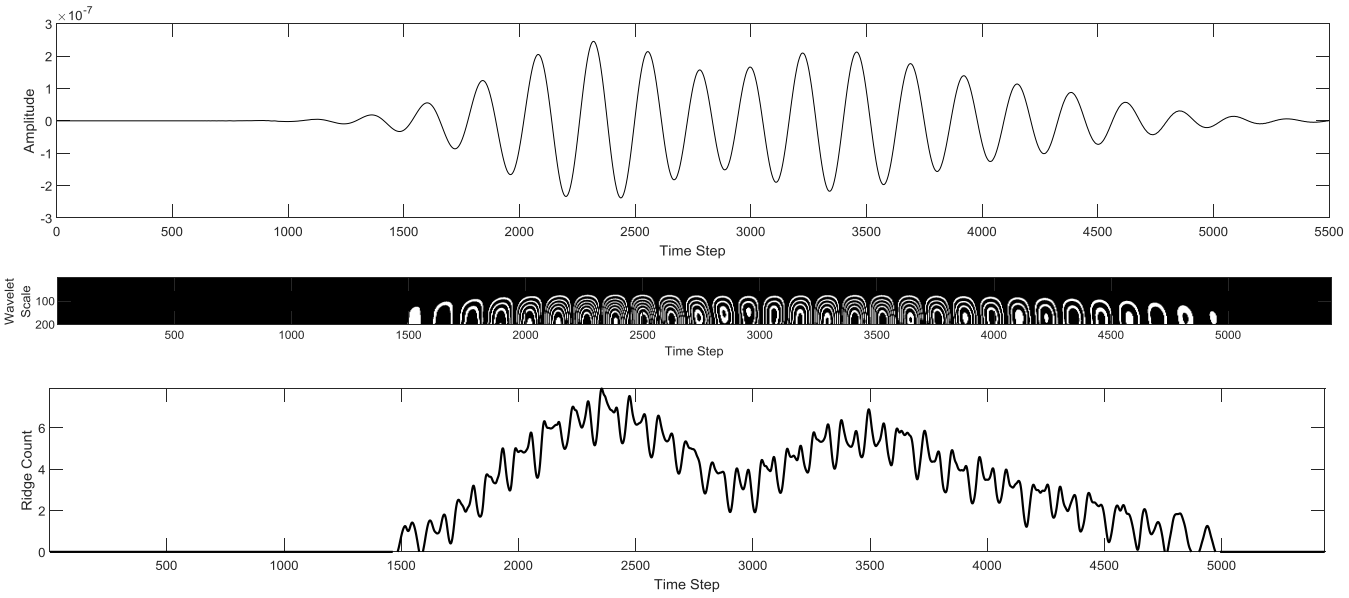

(b) (Top) The time domain plot of the second pulse in the received signal for the 10 GHz frequency simulation. (Middle) The set of fingerprints generated for this segment of signal is shown directly below the time domain plot. (Bottom) A plot of the ridge count feature for the set fingerprints.

FIGURE 9. Plots of the received pulses for NLOS simulations using (a) 5 GHz and (b) 10 GHz center frequencies, highlighting the increased complexity of scattering artifacts at higher frequencies.

full packets to contain a high number of sparse pixel density areas. For example, in one pre-transmission 50 μs OFDM signal, our automatic detection algorithm identified approximately 200 such regions. Therefore, in an analysis of transmissions lasting tens of seconds, one may expect to observe several thousand exclusively high frequency content areas. If an automated system could monitor the existence of content in the high scale areas of a set of fingerprints and track the regularity of such instances over time, it should be able to recognize potential transient occlusion events as they are about to occur in real time. This could be achieved by setting thresholds to alert a user when the number of solely low wavelet scale fingerprint areas drops by increments of 25%, so that when roughly 75% of the expected areas have disappeared over a set amount of time, the system can declare with high confidence that a transmission is being occluded

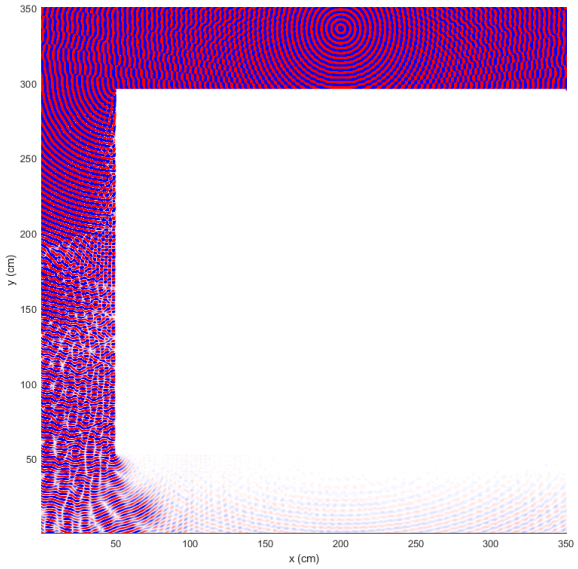

FIGURE 10. The visualization of the z-component of the electric field during the simulation of scattering from a vehicle scenario at time step $t = 7500$.

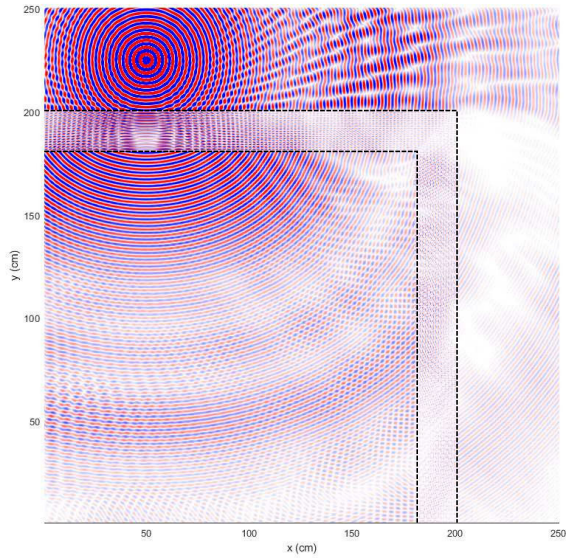

FIGURE 11. The visualization of the z-component of the electric field during the simulation of scattering from a building corner at time step $t = 7500$.

by a scatterer in the environment. A proposed rudimentary framework for predicting/determining the probable the level of signal occlusion is provided in Table 2, while the pseudocode for a real-time detection system is provided in Algorithm 1.

In our analysis of transient occlusion event simulations, we found that signals occluded by buildings were impacted less than those occluded by vehicles. In addition to examining the scattering effects resulting from interactions with urban environments, we also compared the magnitudes of the occluded signals to those of the corresponding LOS simulations. The magnitude of the received signal before and after the Tx node moved around the corner of the building differed by less than 45 dB, while the magnitude of the received signal before and after the Tx node was obstructed by a truck differed by roughly 150 dB. This indicates that the arrival and departure of vehicles and other metal bodies within a device's environment will have a stronger impact on its ability to receive and transmit information effectively than will, to some extent, the movement of a node around a building corner.

One main advantage of implementing the DWFP to detect transient occlusion events in real-world military scenarios is that it provides a means of making an informed decision about the practicality of continuing jamming efforts, thereby preserving battery power and energy expenditure. Rather than continuing to cause interference to a target node that may no longer be transmitting, our proposed method would allow the jammer to gauge the efficacy of its electronic attack efforts and suspend jamming if it is no longer necessary. In commercial scenarios, incorporating our proposed algorithms into CR devices would enable a node to refrain from causing potential interference to other communications links by evaluating the veracity of an apparent vacancy in the channel. This would result in fewer interruptions to the primary user's service. For devices equipped with edge computing

TABLE 2. Proposed basic framework for predicting the probable the level of signal occlusion.

Expected sparse regions observed	Predicted occlusion
$0\% \leq x < 25\%$	Full occlusion
$25\% \leq x < 50\%$	Partial occlusion
$50\% \leq x < 75\%$	Slight occlusion
$75\% \leq x \leq 100\%$	No occlusion

Algorithm 1 Transient Occlusion Event Detection

for *iteration* $i = 1, 2, \ldots$ **do**
  Record transmissions on center frequency f for T time steps
  Apply the DWFP algorithm to the time-domain waveform
  Calculate the pixel density of $I(a, T)$ for the highest wavelet scale band
  Run the sparse region detection algorithm
  Record the number of identified sparse regions S_i
  Calculate $(S_i)/(S_{i-1})$
  if $(S_i)/(S_{i-1}) \leq 0.75$ **then**
    Notify user of potential occlusion event
    If previous iterations are available, calculate $(S_i)/(S_{i-n})$ for $n = 2, 3$ to determine degree of occlusion as defined in Table 2
  else if $(S_i)/(S_{i-1}) > 0.75$ **then**
    No signal occlusion detected, continue to next iteration
  end if
end for

capabilities, our proposed algorithms could be incorporated into nodes of a decentralized network, enabling an exchange of information about transient occlusion events in the local area between neighboring nodes on an intermittent basis and providing individual nodes with a better understanding of the larger environment. One limitation of our work is that our study concentrates on signals that do not utilize a frequency hopping based protocol, so our proposed framework would require some modifications to be made for practical use in instances where the target network employs a frequency hopping spread spectrum protocol. One of the main challenges that will be encountered in the real-world implementation of our occlusion detection algorithm will be amassing a training dataset composed of signals collected in urban environments, where the set of scatterers represented within the data exhibits a realistic level of variation. This would have to include different types of vehicles, ranging from small passenger cars to large delivery trucks, and buildings composed of a wider array of materials, with varying levels of ambient noise and under different weather conditions.

VIII. CONCLUSION AND FUTURE WORK

We have modelled the propagation of 9 GHz frequency signals around vehicles and buildings, since these are the most common elements present in urban environments that will lead to complex signal scattering. Scenarios with temporary hidden node situations, which we termed transient occlusion events, were simulated using a high performance computing cluster and were compared to scenarios where a LOS transmission event was concluded. Sets of fingerprints generated from signals recorded in 3D FDTD simulations of the two different types of situations were compared, and features in the fingerprints corresponding to occlusion of a transmitted signal by a vehicle or a building were identified. The differences we identified between the pixel density feature in the sets of fingerprints resulting from transient occlusion events and in those resulting from LOS transmission events have promise to be used with machine learning algorithms to automate the detection of hidden nodes and to provide an understanding of node behavior in an urban environment. When combined with knowledge of the existence of scatterers such as vehicles and buildings in the immediate neighborhood of a device, this information may be instrumental in determining the likelihood of obstructed vs. concluded transmissions in both civilian and military applications.

Future work will focus largely on obtaining an extensive set of experimental data related to transient occlusion events. Refining and implementing the automatic occlusion event detection framework we have proposed through the incorporation of experimental data would facilitate the development of an automatic system for real-time occlusion detection and prediction. Additional work might also include developing and executing simulations in which the nodes and various scatterers moved in a realistic path through a large computational space. This might be accomplished by designing the simulation environment such that a small area of the space containing the node moves in a sliding three dimensional window through the full space, so that only a localized portion of the grid would be updated at each time step. This implementation of the FDTD method could allow for a larger simulation environment to be modelled while also keeping the computational expense to a minimum. Real-world data mirroring these models could be obtained and analyzed in tandem with simulation results to explain various features observed in the recorded signals and to obtain a more complete understanding of how mobility impacts received signal strength, path loss levels, and the behavior of the scattering environment.

ACKNOWLEDGMENT

The authors would like to thank Bryan Nousain for many helpful discussions and also would like to thank William & Mary Research Computing for providing computational resources and/or technical support that have contributed to the results reported within this work (https://www.wm.edu/it/rc).

REFERENCES

[1] M. Matalatala Tamasala, S. Shikhantsov, M. Deruyck, E. Tanghe, D. Plets, S. K. Goudos, L. Martens, and W. Joseph, "Combined ray-tracing/FDTD and network planner methods for the design of massive MIMO networks," *IEEE Access*, vol. 8, pp. 206371–206387, 2020.

[2] S. Sun, G. R. MacCartney, and T. S. Rappaport, "A novel millimeter-wave channel simulator and applications for 5G wireless communications," in *Proc. IEEE Int. Conf. Commun. (ICC)*, Paris, France, May 2017, pp. 1–7.

[3] T. S. Rappaport, Y. Xing, G. R. MacCartney, A. F. Molisch, E. Mellios, and J. Zhang, "Overview of millimeter wave communications for fifth-generation (5G) wireless networks—With a focus on propagation models," *IEEE Trans. Antennas Propag.*, vol. 65, no. 12, pp. 6213–6230, Dec. 2017.

[4] J. Li, B. Ai, R. He, M. Yang, Z. Zhong, and Y. Hao, "A cluster-based channel model for massive MIMO communications in indoor hotspot scenarios," *IEEE Trans. Wireless Commun.*, vol. 18, no. 8, pp. 3856–3870, Aug. 2019.

[5] J. Ryan, G. R. MacCartney, and T. S. Rappaport, "Indoor office wideband penetration loss measurements at 73 GHz," in *Proc. IEEE Int. Conf. Commun. Workshops (ICC Workshops)*, Paris, France, May 2017, pp. 228–233.

[6] L. Csurgai-Horváth, B. Horváth, I. Rieger, J. Kertész, and B. Adjei-Frimpong, "Indoor propagation measurements for 5G networks," in *Proc. 11th Int. Symp. Commun. Syst., Netw. Digit. Signal Process. (CSNDSP)*, Budapest, Hungary, Jul. 2018, pp. 1–5.

[7] B. Adjei-Frimpong and L. Csurgai-Horvath, "Q-band indoor propagation modelling and measurements for 5G," in *Proc. Eur. Microw. Conf. Central Eur. (EuMCE)*, Prague, Czech Republic, May 2019, pp. 141–144.

[8] Y. Zhang, J. Wen, G. Yang, Z. He, and J. Wang, "Path loss prediction based on machine learning: Principle, method, and data expansion," *Appl. Sci.*, vol. 9, no. 9, p. 1908, May 2019.

[9] K. Y. Yazdandoost and I. Laakso, "Numerical modeling of electromagnetic field exposure from 5G mobile communications at 10 GHZ," *Prog. Electromagn. Res. M*, vol. 72, pp. 61–67, 2018.

[10] M. Bonato, L. Dossi, E. Chiaramello, S. Fiocchi, S. Gallucci, G. Tognola, P. Ravazzani, and M. Parazzini, "Human RF-EMF exposure assessment due to access point in incoming 5G indoor scenario," *IEEE J. Electromagn., RF Microw. Med. Biol.*, vol. 5, no. 3, pp. 269–276, Sep. 2021.

[11] S. Shikhantsov, A. Thielens, G. Vermeeren, E. Tanghe, P. Demeester, L. Martens, G. Torfs, and W. Joseph, "Hybrid ray-tracing/FDTD method for human exposure evaluation of a massive MIMO technology in an industrial indoor environment," *IEEE Access*, vol. 7, pp. 21020–21031, 2019.

[12] S. Bakirtzis, T. Hashimoto, and C. D. Sarris, "FDTD-based diffuse scattering and transmission models for ray tracing of millimeter-wave communication systems," *IEEE Trans. Antennas Propag.*, vol. 69, no. 6, pp. 3389–3398, Jun. 2021.

[13] M. Yamagishi, T. Hikage, M. Sasaki, M. Nakamura, and Y. Takatori, "FDTD-based numerical estimation of human body blockage characteristics in 26 GHz band indoor propagation," in *Proc. 48th Eur. Microwave Conf. (EuMC)*, Madrid, Spain, pp. 878–881, 2018.
[14] S. Nagamoto and M. Omiya, "Highly precise prediction of 28 GHz indoor radio wave propagation characteristics in an office environment for design of 5G wireless networks," in *Proc. IEEE REGION 10 Conf. (TENCON)*, Nov. 2020, pp. 113–116.
[15] K. Saito and M. Omiya, "Predicting outdoor angular characteristics and power distribution of wireless LAN signal leaking from an office building," in *Proc. Int. Symp. Antennas Propag. (ISAP)*, Xi'an, China, Oct. 2019, pp. 1–3.
[16] J. Pardo, G. Ramírez, and D. Rodríguez-Duarte, "Site specific indoor propagation assessment in a 802.11ac WLAN by site survey and ray tracing simulation," in *Proc. IEEE-APS Top. Conf. Antennas Propag. Wireless Commun. (APWC)*, Cartagena, Colombia, Sep. 2018, pp. 936–939.
[17] C. Wang, J. Bian, J. Sun, W. Zhang, and M. Zhang, "A survey of 5G channel measurements and models," *IEEE Commun. Surveys Tuts.*, vol. 20, no. 4, pp. 3142–3168, 4th Quart., 2018.
[18] D. He, B. Ai, K. Guan, L. Wang, Z. Zhong, and T. Kürner, "The design and applications of high-performance ray-tracing simulation platform for 5G and beyond wireless communications: A tutorial," *IEEE Commun. Surveys Tuts.*, vol. 21, no. 1, pp. 10–27, 1st Quart., 2019.
[19] J. Zhang, E. Björnson, M. Matthaiou, D. W. K. Ng, H. Yang, and D. J. Love, "Guest editorial special issue on multiple antenna technologies for beyond 5G—Part II," *IEEE J. Sel. Areas Commun.*, vol. 38, no. 9, pp. 1941–1944, Sep. 2020.
[20] M. K. Hinders, *Intelligent Feature Selection for Machine Learning Using the Dynamic Wavelet Fingerprint*. Cham, Switzerland: Springer, 2020.
[21] J. Yli-Kaakinen, T. Levanen, A. Palin, M. Renfors, and M. Valkama, "Generalized fast-convolution-based filtered-OFDM: Techniques and application to 5G new radio," *IEEE Trans. Signal Process.*, vol. 68, pp. 1213–1228, 2020.
[22] J. Yli-Kaakinen, A. Loulou, T. Levanen, K. Pajukoski, A. Palin, M. Renfors, and M. Valkama, "Frequency-domain signal processing for spectrally-enhanced CP-OFDM waveforms in 5G new radio," *IEEE Trans. Wireless Commun.*, vol. 20, no. 10, pp. 6867–6883, Oct. 2021.
[23] A. C. M. Austin, M. J. Neve, and G. B. Rowe, "Modeling propagation in multifloor buildings using the FDTD method," *IEEE Trans. Antennas Propag.*, vol. 59, no. 11, pp. 4239–4246, Nov. 2011.
[24] P. Series, *Propagation Data and Prediction Methods for the Planning of Indoor Radio Communication Systems and Radio Local Area Networks in the Frequency Range 900 MHz to 100 GHz*, document P.1238-7, Recommendation ITU-R, Feb. 2012.
[25] I. Cuiñas and M. G. Sánchez, "Permittivity and conductivity measurements of building materials at 5.8 GHz and 41.5 GHz," *Wireless Pers. Commun.*, vol. 20, no. 1, pp. 93–100, Jan. 2002.
[26] J. Bingham and M. Hinders, "Lamb wave pipe coating disbond detection using the dynamic wavelet fingerprinting technique," in *Review of Progress in Quantitative Nondestructive Evaluation*, vol. 29. New York, NY, USA: AIP Press, Feb. 2010, pp. 615–622.
[27] C. Bertoncini, K. Rudd, B. Nousain, and M. Hinders, "Wavelet fingerprinting of radio-frequency identification (RFID) tags," *IEEE Trans. Ind. Electron.*, vol. 59, no. 12, pp. 4843–4850, Dec. 2012.
[28] S. L. Kirn and M. K. Hinders, "Dynamic wavelet fingerprint for differentiation of tweet storm types," *Social Netw. Anal. Mining*, vol. 10, no. 1, pp. 1–31, Dec. 2020.
[29] S. L. Kirn and M. K. Hinders, "Bayesian identification of bots using temporal analysis of tweet storms," *Social Netw. Anal. Mining*, vol. 11, no. 1, pp. 1–17, Dec. 2021.
[30] E. D. Skinner, S. L. Kirn, and M. K. Hinders, "Development of underwater beacon for Arctic through-ice communication via satellite," *Cold Regions Sci. Technol.*, vol. 160, pp. 58–79, Apr. 2019.
[31] M. Marcus and B. Pattan, "Millimeter wave propagation: Spectrum management implications," *IEEE Microw. Mag.*, vol. 6, no. 2, pp. 54–62, Jun. 2005.
[32] J. Hou, *Ultrasonic Signal Detection and Recognition Using Dynamic Wavelet Fingerprints*. London, U.K. : William, 2004.

MARGARET M. ROONEY received the B.S. degree in mathematics from St. John's University, Queens, NY, USA, and the M.S. and Ph.D. degrees in applied science from William & Mary, Williamsburg, VA, USA.

She is currently a Research Mathematician with the U.S. Naval Research Laboratory, Tactical Electronic Warfare Division, Washington, DC, USA. Her research interests include the application of various machine learning techniques to device identification and threat detection in densely populated wireless networks, characterization of the interactions between high frequency radio waves and the environment, machine learning, deep reinforcement learning cognitive radio, and wireless communications.

Dr. Rooney was a recipient of the Naval Research Laboratory Jerome and Isabella Karle Distinguished Scholar Fellowship, in 2022.

MARK K. HINDERS received the B.S., M.S., and Ph.D. degrees in aerospace and mechanical engineering from Boston University.

He is currently a Professor in applied science with William & Mary. Before coming to Williamsburg, he was a Senior Scientist with the Massachusetts Technological Laboratory Inc., and also a Research Assistant Professor with Boston University. Prior to that, he was an Electromagnetics Research Engineer with the USAF Rome Laboratory, Hanscom AFB, MA, USA. He conducts research in medical imaging, intelligent robotics, security screening, remote sensing, and nondestructive evaluation. He and his students study the interaction of acoustic, ultrasonic, elastic, thermal, electromagnetic and optical waves with materials, and tissues and structures.